Proceedings of ASME Turbo Expo 2012
GT2012
June 11-15, 2012, Copenhagen, Denmark

GT2012-68652

DETERMINATION OF TIME-RESOLVED HEAT TRANSFER COEFFICIENT AND ADIABATIC EFFECTIVENESS WAVEFORMS WITH UNSTEADY FILM COOLING

James L. Rutledge & Jonathan F. McCall
Air Force Institute of Technology
Wright Patterson AFB, OH, USA

ABSTRACT

Traditional hot gas path film cooling characterization involves the use of wind tunnel models to measure the spatial adiabatic effectiveness (η) and heat transfer coefficient (h) distributions. Periodic unsteadiness in the flow, however, causes fluctuations in both η and h. In this paper we present a novel inverse heat transfer methodology that may be used to approximate the $\eta(t)$ and $h(t)$ waveforms. The technique is a modification of the traditional transient heat transfer technique that, with steady flow conditions only, allows the determination of η and h from a single experiment by measuring the surface temperature history as the material changes temperature after sudden immersion in the flow. However, unlike the traditional transient technique, this new algorithm contains no assumption of steadiness in the formulation of the governing differential equations for heat transfer into a semi-infinite slab. The technique was tested by devising arbitrary waveforms for η and h at a point on a film cooled surface and running a computational simulation of an actual experimental model experiencing those flow conditions. The surface temperature history was corrupted with random noise to simulate actual surface temperature measurements and then fed into an algorithm developed here that successfully and consistently approximated the $\eta(t)$ and $h(t)$ waveforms.

INTRODUCTION

Film cooling protects hot gas path components by providing a layer of protective coolant between the surfaces and the hot freestream gas. The film effectively reduces the adiabatic wall temperature, T_{aw}, thereby reducing the driving potential for heat transfer. Film cooling also tends to increase the heat transfer coefficient, h, necessitating prediction or experimental measurement of T_{aw} and h to accurately predict the heat flux into the surface. T_{aw} is nondimensionalized in the form of the adiabatic effectiveness η, defined as

$$\eta = \frac{T_\infty - T_{aw}}{T_\infty - T_c} \tag{1}$$

Eq. (1) facilitates prediction of T_{aw} on a real engine component through measurement on a scaled experimental model at temperatures more convenient in a laboratory setting since η is matched. The net heat flux reduction (NHFR) takes into account the effects on both T_{aw} and h and quantifies the net benefit of film cooling in terms of heat load to a component with T_s held at some acceptable temperature [1]:

$$\Delta q_r \equiv 1 - \frac{q_f''}{q_0''} = 1 - \frac{h(T_{aw} - T_s)}{h_0(T_\infty - T_s)} \tag{2}$$

The h in Eq. (2) is often denoted h_f to emphasize that it is measured with film cooling, but we shall dispense with the subscript in the present paper. The heat transfer coefficient without film cooling is represented by h_0. Some algebraic manipulation will show:

$$\Delta q_r = 1 - \frac{h}{h_0}\left(1 - \frac{\eta}{\phi}\right) \tag{3}$$

where ϕ is the nondimensionalized local surface temperature of the engine component, or overall effectiveness. Typically, ϕ is assumed to be in the vicinity of 0.6 but may be adjusted accordingly to correspond to the desired metal temperature [1]. If any unsteadiness is present that would cause fluctuations in η or h, the NHFR is more meaningful in the time averaged sense. Reference [2] showed that the time averaged NHFR may be written

$$\overline{\Delta q_r} = 1 - \frac{\bar{h}}{h_0}\left(1 - \frac{\bar{\eta}}{\phi}\right) + \frac{\overline{h'\eta'}}{h_0\phi} \tag{4}$$

with bars indicating time averaged quantities and the primes indicating zero-mean fluctuating components. Direct application of Eq. (4) requires time resolved measurements of h and η, which proves rather difficult. Reference [2] developed a way around this problem by defining a new parameter, γ, that

we will see is easily measureable and takes into account the combined effects of the more difficult parameters to measure:

$$\gamma \equiv \bar{\eta} + \frac{\overline{h'\eta'}}{\bar{h}} \tag{5}$$

Reference [2] calls γ the "unsteady coupled average adiabatic effectiveness." This parameter allows Eq. (4) to be rewritten:

$$\overline{\Delta q_r} = 1 - \frac{\bar{h}}{h_0}\left(1 - \frac{\gamma}{\phi}\right) \tag{6}$$

Reference [2] proved that γ can be determined from the surface temperature on a film cooled model using infrared thermography and the following equation:

$$\gamma = \frac{T_\infty - \overline{T_s}}{T_\infty - T_c} - \frac{\overline{q_f''}}{\bar{h}\left(T_\infty - T_c\right)} - \frac{\overline{h'T_s'}}{\bar{h}\left(T_\infty - T_c\right)} \tag{7}$$

Direct application of Eq. (7) would require time resolved T_s and h measurements as indicated by the last term on the RHS. This term may be kept negligible, however, provided that the heat capacity, ρc, of the model material is sufficiently large that temperature fluctuations in the material are damped to negligible levels. To be precise, the nondimensional parameter that governs the temperature fluctuations is called C, defined as:

$$C = \sqrt{\frac{k\rho c\omega}{2\bar{h}^2}} \tag{8}$$

Reference [2] shows that the magnitude of T_s' is inversely related to C. Such an experiment with large C yields γ and $\bar{h}$, but not $\bar{\eta}$. Since this experimental technique requires only single temperature measurements for both the γ and $\bar{h}$ experiments it naturally does not provide the time resolved waveforms of η and h.

The purpose of the present research is to develop and test an inverse heat transfer methodology to determine the $\eta(t)$ and $h(t)$ waveforms. These waveforms can then be applied directly to Eq. (4) if desired, or examined to yield previously unattainable insight into the interactions between h and η. Additionally, the new methodology allows for determination of both waveforms with a single experiment.

INVERSE HEAT TRANSFER AS APPLIED TO FILM COOLING

Traditional steady film cooling experiments are generally simple enough that they are rarely discussed in terms of inverse heat transfer. Before proceeding to the more complex case of unsteady $\eta(t)$ and $h(t)$, it is instructive to consider how inverse heat transfer techniques apply to the legacy experiments.

A typical "forward" heat transfer problem is one in which a temperature distribution or heat flux (both may be a function of time) is sought from known boundary conditions. With the inverse problem, we normally have the temperature or heat flux data and wish to determine the boundary conditions. This is precisely the case with traditional film cooling experiments.

For example, consider a steady wind tunnel experiment from which we wish to determine η. The heat flux into the model may be written:

$$q = h\left(T_{aw} - T_s\right) \tag{9}$$

or

$$T_{aw} = \frac{q}{h} + T_s \tag{10}$$

Nondimensionalizing Eq. (10) using the definition of η:

$$\eta = \frac{T_\infty - T_s}{T_\infty - T_c} - \frac{q}{h\left(T_\infty - T_c\right)} \tag{11}$$

The determination of η is often desired without prior knowledge of h or an accurate measurement of q. The experiment is thus typically conducted using a nearly adiabatic material so that the second term on the RHS of Eq. (11) is negligible, or at least small enough such that the error due to rough approximations for h and q cause little error in the measurement of η. (Note the similarity between Eqs. (11) and (7) when the last term on the RHS of Eq. (7) is kept small.) The methods used to account for the second term in Eq. (11) are varied. For example, it is common to cover the film cooling holes in the region of interest with tape to determine the influence of conduction by observing the surface temperature, which is different from T_∞ even though the absence of film cooling dictates that $\eta = 0$. In any event, this is a rudimentary use of inverse heat transfer methodologies—the boundary condition, T_{aw}, is determined through a surface temperature measurement that differs slightly from T_{aw}.

Another popular experimental technique that is more recognizable as an inverse heat transfer technique is that developed by Vedula and Metzger [3] and used by such researchers as Ekkad et al. [4]. In this methodology, a film cooled model is thermally soaked to a uniform and known temperature, T_i. The model is then suddenly exposed to flow conditions, resulting in a step change in boundary conditions. The transient surface temperature distribution is measured and the boundary conditions, T_{aw} and h, are sought. Because the heat transfer is transient, Fourier's law of conduction must be applied to the problem. If the model and time length of the experiment is designed properly, one may assume that the conduction is locally one-dimensional and that the model behaves as a semi-infinite slab (the thermal wave never penetrates the material, i.e. $\sqrt{\alpha t_{\max}} << thickness$). In this case, conduction behaves according to the following differential equation with the indicated initial condition and boundary values:

$$k\frac{\partial^2 T}{\partial x^2} = \rho c\frac{\partial T}{\partial t} \tag{12}$$

$$-k\left.\frac{\partial T}{\partial x}\right|_{x=0} = h\left(T_{aw} - T_s(t)\right) \tag{13}$$

$$\left.T\right|_{t=0} = T_i \tag{14}$$

which implies: $$T\big|_{x\to\infty} = T_i \tag{15}$$

The convective heat flux boundary condition contains the unknown parameters (h and T_{aw}) that are sought through knowledge of the resulting surface temperature as a function of time. Designing the experiment such that the model may be treated as a semi-infinite slab with a step change in boundary condition as above allows the use of a classic analytical solution to the above differential equation. The solution for the surface temperature response is available in such heat transfer texts as Ref. [5]:

$$\frac{T_s - T_i}{T_{aw} - T_i} = 1 - \exp\left(\frac{h^2\alpha t}{k^2}\right)\operatorname{erfc}\left(\frac{h\sqrt{\alpha t}}{k}\right) \tag{16}$$

In theory, only two surface temperature measurements need be recorded at different times after initiation of the experiment. Eq. (16) applies at both times and the two unknown parameters, h and T_{aw}, can be determined. More accuracy can be obtained through a least squares curve fit to many temperature measurements forming a time history of surface temperature.

As shown by its development, Eq. (16) is not applicable if there is any unsteadiness in either h or T_{aw}. In the present study, we develop an inverse heat transfer technique not to simply determine two values, h and T_{aw}, but rather the functions $h(t)$ and $T_{aw}(t)$. The boundary condition of Eq. (13) is replaced with

$$-k\frac{\partial T}{\partial x}\bigg|_{x=0} = h(t)\left(T_{aw}(t) - T_s(t)\right) \tag{17}$$

where $h(t)$ and $T_{aw}(t)$ are unknown periodic functions. No such classic analytical solution is known to exist for arbitrary waveforms of $h(t)$ and $T_{aw}(t)$. Texts such as Ref. [6] present general solution methodologies for inverse heat transfer problems, but this problem is complicated by the absence of an analytical solution to the forward problem. This challenge necessitated the development of a new inverse heat transfer technique.

THE INVERSE FLUX SOLVER FOR ARBITRARY WAVEFORMS (IFSAW)

The methodology we developed to determine the periodic $h(t)$ and $T_{aw}(t)$ waveforms from a surface temperature time history is described here. The conduct of the experiment itself is quite similar to that described in Ref. [4]; however, the data reduction algorithm differs markedly. In a later section, the algorithm is used to step through several sample cases.

1. Cold soak an experimental model to a uniform and known temperature. A convenient temperature is the coolant temperature. This way, unsteady coolant can run through the cold soaked model prior to test initiation, reducing the number of events that must occur to begin the experiment.
2. Initiate the test by suddenly exposing the film cooled model to a freestream flow at a different, but known, temperature.
3. Measure the spatial surface temperature distribution as a function of time. The use of an infrared camera is a convenient way to do this, but the temperature data must be acquired fast enough to properly resolve the unsteady surface temperature response—this was not a criterion for the experimental equipment required for steady h and T_{aw}. The calculations described herein are then performed at each individual pixel falling on the model surface. Alternatively, liquid crystals or discrete thermocouples could be used to provide surface temperature histories. Conclude the measurements before the thermal wave penetrates the thickness of the model material, i.e. $\sqrt{\alpha t_{\max}} << thickness$.
4. We now seek the solution to the forward heat transfer problem for the surface heat flux. The surface temperature history is a Dirichlet boundary condition. The differential equation with associated boundary conditions is then:

$$k\frac{\partial^2 T}{\partial x^2} = \rho c\frac{\partial T}{\partial t} \tag{18}$$

$$T\big|_{x=0} = T_s(t) \tag{19}$$

$$T\big|_{t=0} = T_i \tag{20}$$

which implies: $$T\big|_{x\to\infty} = T_i \tag{21}$$

Note that only the second boundary condition, Eq. (19), differs from the inverse problem with the boundary condition given by Eq. (13). The boundary conditions are known following the experiment, making this step a forward heat transfer problem. The first step in solving this forward problem is to filter the temperature data. Random noise in the data can have the effect of making the solution appear to have non-physical fluctuations in the heat flux. The authors found that third order Savitzky-Golay filtering [7] is efficient and effective. Care must be taken in the application of the filter to ensure that the highest frequency fluctuations in η and h are not lost. The noise in the temperature data may very well limit this frequency. The authors experimented with two distinct approaches to solving the forward heat transfer problem:

Computational Heat Transfer Simulation

In this approach, a simple time-marching one-dimensional second order accurate numerical heat transfer solver was written. The length of the computational domain should be selected such that it is an order of magnitude longer than $\sqrt{\alpha t_{\max}}$ to ensure that indeed a semi-infinite slab is modeled. The temporal and spatial discretization should be selected such that the von Neumann stability requirement is satisfied [8]:

$$\frac{\alpha\Delta t}{(\Delta x)^2} \le \frac{1}{2} \tag{22}$$

At the surface, the temperature is simply set to the filtered experimental temperature data, which may be interpolated to provide sufficiently small Δt. Equation (18) is solved within the domain using an adiabatic boundary condition, $\frac{\partial T}{\partial x}=0$, at the end of the domain. It is wise to ensure that the domain is long enough by recording the temperature at the end of the domain at the end of the simulation. This temperature should not differ significantly from the initial temperature. At each time step, the critical output is the surface heat flux, calculated from the surface temperature gradient.

$$q_s(t) = -k\left.\frac{\partial T}{\partial x}\right|_{x=0} \tag{23}$$

Analytical Solution for Heat Flux

As an alternative to relying on a computational simulation to find the surface heat flux from the Dirichlet boundary condition, $T_s(t)$, an analytical solution exists for Eqs. (18) through (21). Reference [9] presents the solution $T(x,t)$ for an arbitrary surface boundary condition $T_s(t)$, after the semi-infinite slab is initially at a uniform temperature as:

$$T(x,t)-T_i = \frac{x}{2\sqrt{\pi\alpha}}\int_0^t f(\lambda)\frac{e^{-x^2/(4\alpha(t-\lambda))}}{(t-\lambda)^{3/2}}d\lambda \tag{24}$$

where

$$f(t) = T_s(t)-T_i \tag{25}$$

The temperature gradient is then found through differentiation and ultimately, the surface heat flux may be written:

$$q_s(t) = \lim_{x\to 0}\frac{-2k}{x\sqrt{\pi}}\int_{x/(2\sqrt{\alpha t})}^{\infty} f\left(t-\frac{x^2}{4\alpha\mu^2}\right)e^{-\mu^2}\left(1-2\mu^2\right)d\mu \tag{26}$$

Because the function $f(t)$ is discrete, a numerical integration scheme must be employed.

Both methods described above to calculate $q_s(t)$ were confirmed to yield equivalent results through testing. The selection of either the analytical solution, which involves an improper integral, or the computational simulation is a choice to be made by the user and may be dependent on computational resources.

5. With $q_s(t)$ now in hand, we wish to find periodic $T_{aw}(t)$ and $h(t)$ functions that are least squares fits to

$$q_s(t) = h(t)\left(T_{aw}(t)-T_s(t)\right) \tag{27}$$

Both $q_s(t)$ and $T_s(t)$ are now known. We may use truncated Fourier series to approximate the periodic $T_{aw}(t)$ and $h(t)$ functions:

$$h(t) = \frac{\hat{h}_0}{2}+\sum_{n=1}^{N}\left(\hat{h}_n\cos\frac{n\pi t}{L}+\tilde{h}_n\sin\frac{n\pi t}{L}\right) \tag{28}$$

$$T_{aw}(t) = \frac{\hat{T}_0}{2}+\sum_{n=1}^{N}\left(\hat{T}_n\cos\frac{n\pi t}{L}+\tilde{T}_n\sin\frac{n\pi t}{L}\right) \tag{29}$$

In the above formulation, both waveforms are written with the same number of parameters, $2N+1$, but there is no requirement to do so. Since it is likely that the same phenomenon that causes fluctuations in T_{aw} also causes fluctuations in h, it is entirely reasonable to use the same number of terms to approximate each parameter. Also note that both waveforms written above use the same period length, L, for the same physical reasoning. Alternatively, different period lengths may be used in Eqs. (28) and (29); however, as will be explained below, the implementation of this inverse heat transfer methodology is facilitated somewhat by this valid assumption of common period length.

We wish to minimize ε, the sum of the square of the errors, across all N_P data points by optimizing L and the vectors $\hat{h}_n$, $\tilde{h}_n$, $\hat{T}_n$, $\tilde{T}_n$ in:

$$\varepsilon = \sum_{i=1}^{N_P}\left[\begin{array}{l} q_s(t_i)-\left(\frac{\hat{h}_0}{2}+\sum_{n=1}^{N}\left(\hat{h}_n\cos\frac{n\pi t_i}{L}+\tilde{h}_n\sin\frac{n\pi t_i}{L}\right)\right) \\ \times\left(\left(\frac{\hat{T}_0}{2}+\sum_{n=1}^{N}\left(\hat{T}_n\cos\frac{n\pi t_i}{L}+\tilde{T}_n\sin\frac{n\pi t_i}{L}\right)\right)-T_s(t_i)\right)\end{array}\right]^2 \tag{30}$$

Such an optimization procedure may be achieved through algorithms such as the Levenberg-Marquardt or trust-region methods. We have experienced good success using the trust-region reflective algorithm implemented within Matlab. The choice of N, relating to the number of terms in the Fourier series depends on the fidelity with which one wishes to approximate the $T_{aw}(t)$ and $h(t)$ waveforms. For the experimentation used in this paper, we have used $N = 13$, thereby optimizing on a total of 55 parameters-- $2N+1$ for each waveform and the period length, L. The optimization routine is quite insensitive to the initial guesses on the $\hat{h}_n$, $\tilde{h}_n$, $\hat{T}_n$ and $\tilde{T}_n$; however, a poor initial guess of L can result in failure to optimize. In many practical cases, the experimentalist may have a good idea of the lowest frequency expected in the waveforms. It may be the frequency of coolant pulsation or it may be the blade passing frequency. Nevertheless, our methodology requires no such a priori knowledge.

The frequency content of the raw measured temperature data may be automatically determined through an appropriate application of a fast Fourier transform (FFT). Savitzky-Golay filtering may be used once again on the temperature data, but this time with a moving average spanning many cycles. This long-time moving average may be subtracted from the raw temperature data to observe the fluctuating component of the surface temperature. An FFT may then be performed on these temperature fluctuations to produce the single-sided amplitude spectrum. Of the multiple peaks we would expect to see, we desire the lowest frequency peak. A number of techniques exist to automatically locate this peak. One simple method we use is an algorithm to identify all

local maxima that fall above 3 standard deviations above the mean of the amplitude spectrum. Of those identified peaks, we select the one at the lowest frequency. Inverting this frequency provides a good initial guess to optimize on the period length, L. In any event, this is only a method to provide an initial guess to be refined during optimization; failure to optimize would indicate a poor initial guess thereby removing the impact of subjectivity in this estimate.

If different period lengths, L, are used in Eqs. (28) and (29), then the aforementioned technique to acquire an initial guess would still only provide a single initial guess. A more robust optimization routine that is less sensitive to the initial guess on the period length might need to be used instead. Nevertheless, as mentioned earlier, the flow physics are probably such that the same phenomenon is responsible for fluctuations in both h and T_{aw} so that L is the same for each.

A summary of the IFSAW algorithm as described above is presented in Figure 1.

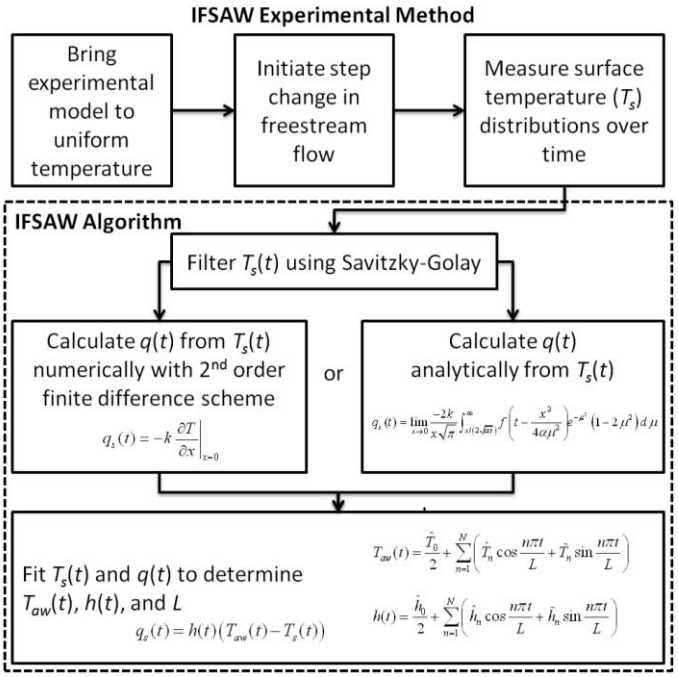

Figure 1: FLOWCHART SHOWING STEPS TO CONDUCT EXPERIMENT AND REDUCE DATA IN ACCORDANCE WITH IFSAW ALGORITHM

ALGORITHM TESTING METHODOLOGY

To test the IFSAW algorithm, it would be inappropriate to proceed immediately to a physical laboratory experiment. No other technique to reliably determine the h and η waveforms is known to exist, so it would be difficult at this point to verify that the resulting waveforms are in fact, correct approximations for the true waveforms. As discussed in Ref [2], the heat capacity, ρc, of the model can cause such dampening of the surface temperature fluctuations with periodic steady-state experiments that even determination of $\overline{\eta}$ is extremely difficult with that method, let alone the actual waveforms. Future experimental work with very slow fluctuations, however, may be able to test the algorithm.

Test Overview

For testing the algorithm, we thus selected a computational simulation of the experiment. We contrived a variety of h and η waveforms, allowing us to test the robustness of the IFSAW algorithm. A good data reduction algorithm must be able to handle not only the foreseen, but also the unexpected as the algorithm may be applied to handle unsteady heat transfer situations created by more than just simple coolant pulsing with a single frequency component. The contrived h and η waveforms were then input to a one-dimensional transient heat transfer simulator to determine the true surface temperature history following initiation of the transient experiment. The output of this simulation is termed "actual" data and would be impossible to physically measure—it represents the actual physical state of the test article under the prescribed conditions. Random error was then added to the temperature history to simulate laboratory measurements—this is the "measured" data. The noisy temperature history was then input to the IFSAW algorithm and the resulting waveforms compared to the originals. A summary of the validation procedure used in this study is provided in Figure 2. Details regarding the implementation will follow.

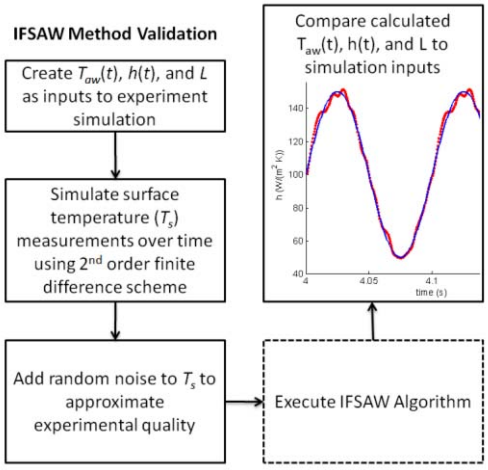

Figure 2: VALIDATION PROCEDURE FLOWCHART

Test Details

A second order accurate finite differencing scheme was created to simulate the experiment. The code is similar to the IFSAW code that determines the surface heat flux from the Dirichlet boundary condition. This test simulator code, however, uses the Robin type surface boundary condition to determine the temperature profile through the slab. This surface boundary condition is given by Eq. (17), repeated here:

$$-k\left.\frac{\partial T}{\partial x}\right|_{x=0} = h(t)\left(T_{aw}(t)-T_s(t)\right) \qquad (17)$$

For the experimental simulation we have prescribed $h(t)$ and $T_{aw}(t)$ through the conversion:

$$T_{aw}(t) = T_\infty - \eta(t)\left(T_\infty - T_c\right) \tag{31}$$

T_∞ and T_c are selected according to what would be expected in the laboratory to simulate a situation in which η varies due to periodic unsteadiness in the coolant blowing rate.* The initial condition of the simulation is the initial temperature of the model. As mentioned above, it is convenient from a practical standpoint to soak the model at the coolant temperature; we have thus selected $T_i = T_c$ for our simulations.

It was critical to ensure that the transient simulation code functions properly. The code was validated using several techniques, including using steady h and η boundary conditions (Eq. (13)), for which a simple analytical solution for the surface temperature history exists (Eq. (16)). In this and all subsequent simulations, we assume the model is made of General Plastics Last-A-Foam FR-7106. The material properties and conditions for the simulation of the experiment are shown in Table 1. For the steady h and η validation case, we chose to simulate $\eta = 0.4$ and $h = 100$ W/(m^2 K). The absolute value of the temperature error from the numerical simulation as compared with the analytical solution is plotted in Figure 3. The largest error is at the beginning of the simulation when temperature gradients, both in time and space, are largest. Here, the error in temperature is a maximum of 0.0039 K at 0.5 ms after initiation.

Table 1: SIMULATED EXPERIMENTAL CONDITIONS AND MATERIAL PROPERTIES

Property or Condition	Value	Source / Rationale
k	0.03 W/(m K)	Property of Last-A-Foam FR-7106; From General Plastics
ρ	96 kg/m^3	Property of Last-A-Foam FR-7106; From General Plastics
c	1260 J/(kg K)	Ref. [10]
T_c	290 K	Easily achievable in lab with a chiller
T_i	290 K	same as Taw- allows coolant to run through the cold soaked model prior to mainstream flow initiation
T_∞	320 K	Easily achievable in lab with flow heater
ε_T	0.1 K	temperature measurement uncertainty with 95% confidence

* Alternative situations can be imagined in which T_∞ and/or T_c depend on time. The impact remains the same, though, in that T_{aw} is a function of time. The time dependent values $T_\infty(t)$ and $T_c(t)$ would then be used in the nondimensionalization of $T_{aw}(t)$ to determine $\eta(t)$.

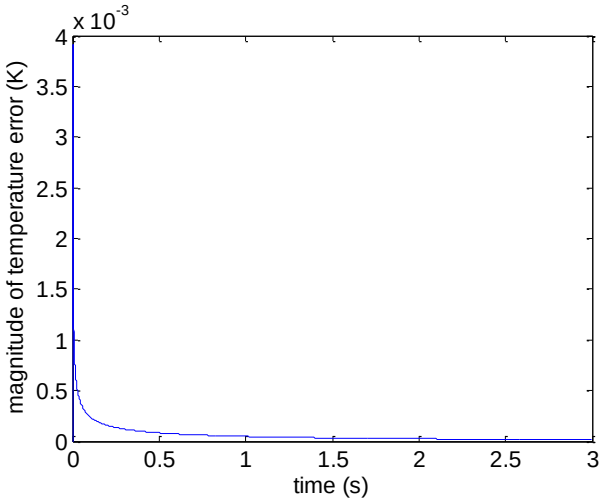

Figure 3: TEMPERATURE ERROR (K) IN NUMERICAL SIMULATION OF EXPERIMENT AS COMPARED WITH ANALYTICAL SOLUTION FOR STEADY *h* AND η.

RESULTS

To demonstrate the IFSAW procedure with a practical example, we selected the following simple waveforms for h and η:

$$h = 100 + 50\sin\left(2\pi \cdot 10t\right) \text{ W/(m}^2\text{K)} \tag{32}$$

$$\eta = 0.4 + 0.3\sin\left(2\pi \cdot 10t\right) \tag{33}$$

These waveforms are in phase; that is, h is high when η is high as is usually the case. The parameters of 10 Hz and $\bar{h} = 100$ W were selected as indicative of a 10x scale wind tunnel experiment roughly matching Reynolds number and nondimensional blade passing frequency order of magnitude with an actual engine (c.f. Ref [11]). The selection of $\bar{\eta} = 0.4$ is reasonable for a location downstream of a film cooling jet (c.f. Ref [11]).

First, for the purposes of testing/demonstrating IFSAW, we ran a numerical simulation of the experiment using the parameters in Table 1. The first 0.5 seconds of the surface temperature response is shown in Figure 4. Although the time step used in the numerical simulation was 10^{-5} seconds, temperature data was saved at 2 kHz, a more realistic laboratory data acquisition rate. We can immediately learn something about the choice of model materials for such an experiment. During these first 0.5 seconds, the temperature rises from 290 K to just over 300 K. This is inconvenient for the experimentalist, who would prefer for the temperature change at the beginning to be less rapid. This is often alleviated through the use of higher heat capacity materials such as acrylic instead of foam. Although fine for the steady film cooling experiments, higher heat capacity results in smaller surface temperature undulations, exacerbating the uncertainty in the ultimate goal of determining the $h(t)$ and $\eta(t)$ waveforms.

Temperature measurement noise is a major hurdle with inverse heat transfer and must be accounted for in simulations of experiments. In order to simulate real imperfect temperature measurements in the laboratory, we added a normally distributed random error with 95% confidence uncertainty of 0.1 K. This noisy data was then filtered using Savitzky-Golay filtering. The original "actual" temperature data along with the simulated "measured" noisy data and finally the filtered data are shown in Figure 5 for a subset of the time period shown in Figure 4. The filter is imperfect, but it cleans up the data well enough for use as the Dirichlet boundary condition to compute the surface heat flux.

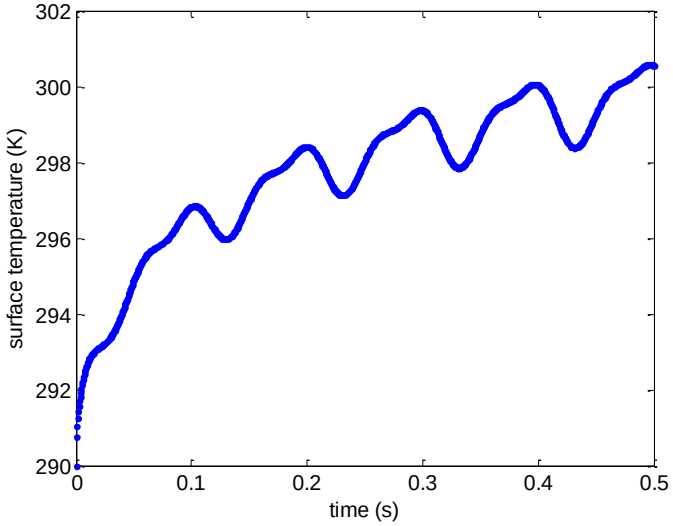

Figure 4: SURFACE TEMPERATURE OVER FIRST 0.5 SEC OF SIMULATED EXPERIMENT WITH $h = 100 + 50\sin(2\pi \cdot 10t)$ **AND** $\eta = 0.4 + 0.3\sin(2\pi \cdot 10t)$

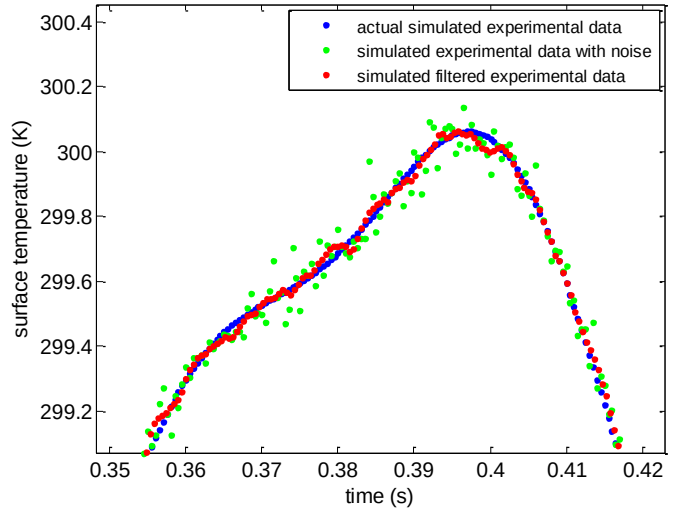

Figure 5: ACTUAL SURFACE TEMPERATURE (BLUE), SIMULATED NOISY MEASURED DATA WITH 0.1 K UNCERTAINTY (GREEN) AND FILTERED DATA (RED). THE FILTERED DATA IS LATER USED TO DETERMINE THE SURFACE HEAT FLUX.

The heat flux was then calculated from the filtered surface temperature history and plotted in Figure 6 along with the actual surface heat flux, provided as an output from the original simulation only for comparison purposes. The influence of measurement noise is apparent, but the least squares fits for the Fourier series approximations for $h(t)$ and $T_{aw}(t)$ will be shown to be quite accurate, particularly by taking a longer set of data than the 0.5 seconds shown here.

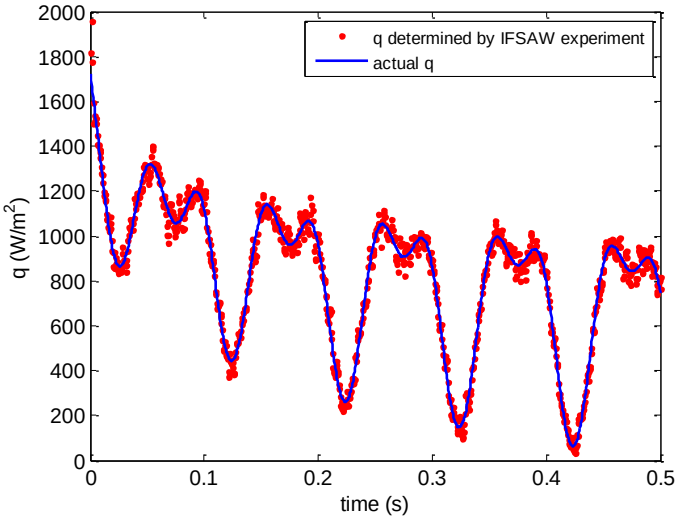

Figure 6: SURFACE HEAT FLUX DETERMINED BY IFSAW ALGORITHM COMPARED TO ACTUAL HEAT FLUX

At this point, we must choose the number of terms we wish to use in the Fourier series approximations (Eqs. (28) and (29)). For this simple contrived example, we know that few terms are required (only 5 of the constants are non-zero); however, we cannot use any a priori knowledge of the form of the result to test the algorithm. Therefore, we used $N = 13$ in Eqs. (28) and (29) for a total of 55 unknown constants to find through optimizing Eq. (30). We found that this technique could provide decent approximations to even the more ill-behaved waveforms to be shown later. The simulation of the present example was run for 20 seconds of physical time and the waveforms output by the IFSAW algorithm are compared to the true waveforms in Figures 7 and 8. The influence of using "too many" terms in the Fourier series is evident; however, the approximations are decent. The approximations can then be used to calculate γ (through Eq. (5)) and $\bar{h}$. These values are compared with the true values in Table 2.

Table 2 also gives the values that would be obtained if one erroneously assumed that h and η are constant and determined those values through a curve fit with Eq. (16). As it turns out, in this case, that curve fit happens to give decent values if we were to assume (again, erroneously) that $\gamma = \eta$ as would be the case with steady film cooling (Eq. (5)). In any event, only the IFSAW data reduction technique yields the time resolved waveforms.

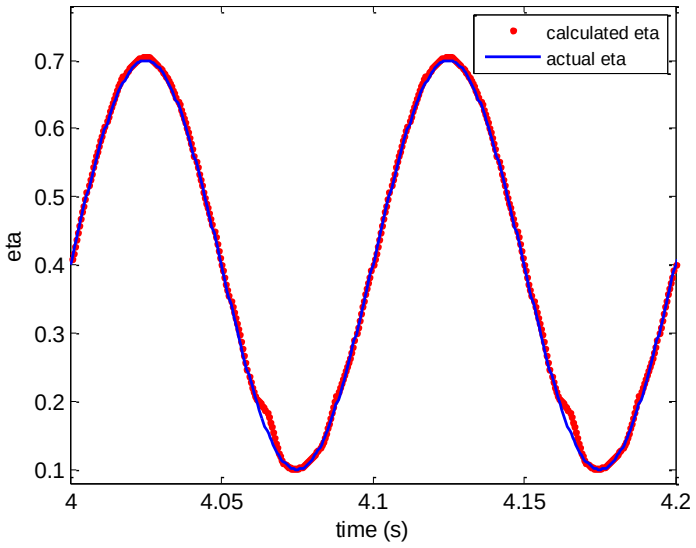

Figure 7: $\eta(t)$ WAVEFORM DETERMINED WITH 20 SECOND SIMULATED EXPERIMENT WITH $h = 100 + 50\sin(2\pi \cdot 10t)$ AND $\eta = 0.4 + 0.3\sin(2\pi \cdot 10t)$

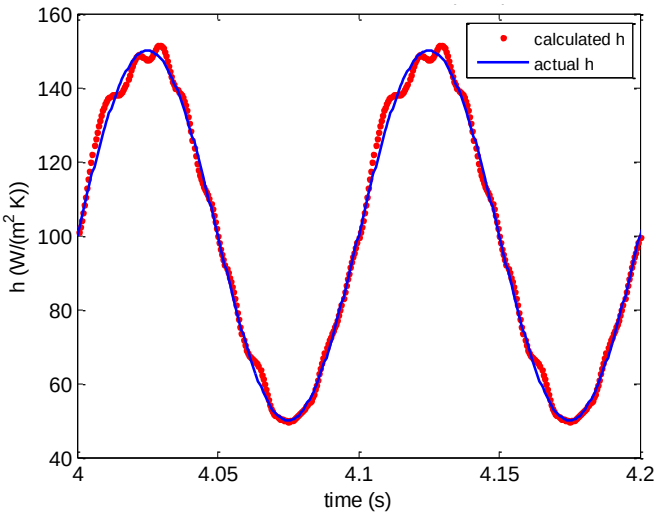

Figure 8: $h(t)$ WAVEFORM DETERMINED WITH 20 SECOND SIMULATED EXPERIMENT WITH $h = 100 + 50\sin(2\pi \cdot 10t)$ AND $\eta = 0.4 + 0.3\sin(2\pi \cdot 10t)$

Table 2: ACTUAL AND CALCULATED FILM COOLING PARAMETERS WITH $h = 100 + 50\sin(2\pi \cdot 10t)$ AND $\eta = 0.4 + 0.3\sin(2\pi \cdot 10t)$ FOLLOWING A 20 SECOND EXPERIMENT

	γ	$\bar{h}$ (W/(m^2 K))
Actual Values	0.4750	100
Values calculated from measurement	0.4785	100.5831
Legacy Technique that Assumes Constant h and η.	0.4670	98.8744

The next set of tested waveforms contains several terms including a triangle wave to test the algorithm with a non-smooth function:

$$h = 100 + 10 \cdot triangle(2\pi \cdot 8t) + 30 \cdot \sin(2\pi \cdot 16t)... \\ +10 \cdot \cos(2\pi \cdot 24t) + 5 \cdot \sin(2\pi \cdot 24t) + 5 \cdot \cos(2\pi \cdot 32t) \quad \text{W/(m}^2\text{K)} \qquad (34)$$

$$\eta = 0.4 + 0.05 \cdot triangle(2\pi \cdot 8t) + 0.2 \cdot \sin(2\pi \cdot 8t)... \\ +0.05 \cdot \sin(2\pi \cdot 40t) + 0.08 \cdot \cos(2\pi \cdot 32t) \qquad (35)$$

Again, the simulated experiment was run for 20 seconds with random temperature uncertainty of 0.1 K. The algorithm properly determined the lowest frequency component to be 8 Hz and produced the results depicted in Figures 9 and 10. The actual value of γ for this condition is $\gamma = 0.4034$ and the actual value of $\bar{h}$ is $\bar{h} = 100$ W/(m^2 K). The values reported by analysis of the simulated measurements are $\gamma = 0.4068$ and $\bar{h} = 100.69$ W/(m^2 K).

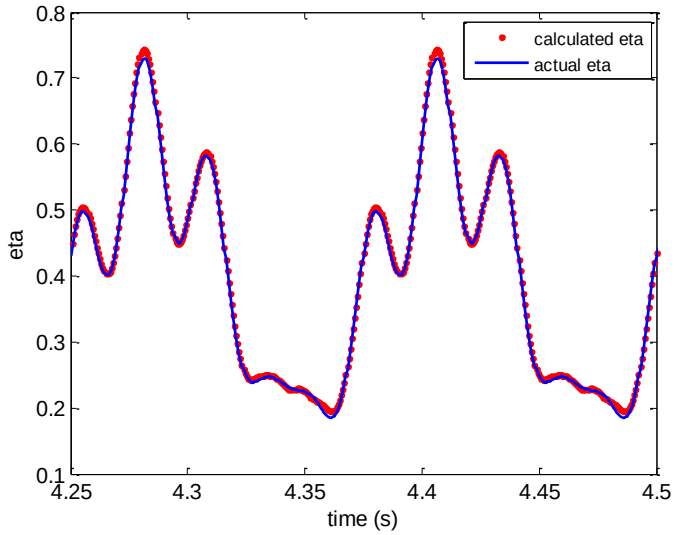

Figure 9: $\eta(t)$ WAVEFORM DETERMINED WITH 20 SECOND SIMULATED EXPERIMENT WITH WAVEFORMS GIVEN BY EQS. (34) AND (35)

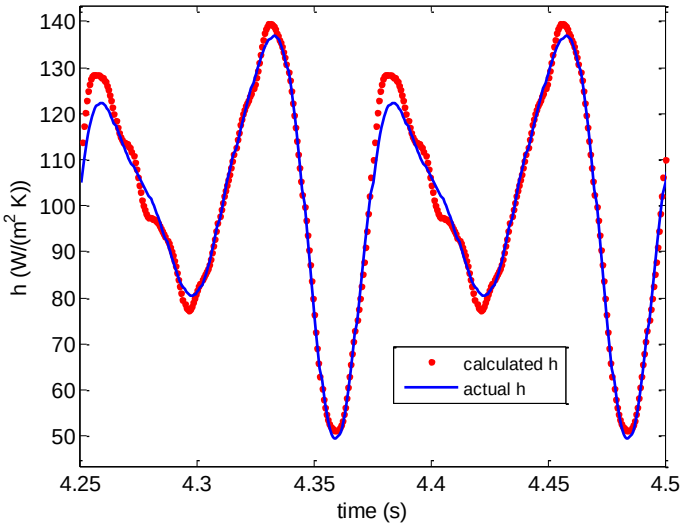

Figure 10: $h(t)$ WAVEFORM DETERMINED WITH 20 SECOND SIMULATED EXPERIMENT WITH WAVEFORMS GIVEN BY EQS. (34) AND (35)

Another 20 second experiment was simulated with the following waveforms:

$$h = 100 + 30 \cdot triangle(2\pi \cdot 8t) + 10 \cdot \sin(2\pi \cdot 16t)... \\ +10 \cdot \cos(2\pi \cdot 24t) + 5 \cdot \sin(2\pi \cdot 24t) + 5 \cdot \cos(2\pi \cdot 32t) \quad \text{W/(m}^2\text{K)} \tag{36}$$

$$\eta = 0.4 + 0.2 \cdot triangle(2\pi \cdot 8t) + 0.04 \cdot \sin(2\pi \cdot 8t)... \\ +0.05 \cdot \sin(2\pi \cdot 40t) + 0.08 \cdot \cos(2\pi \cdot 32t) + 0.01 \cdot \cos(2\pi \cdot 56t) \tag{37}$$

Figures 11 and 12 depict those waveforms and the experimentally determined waveforms. The actual $h(t)$ waveform contains a sharp discontinuity in its first derivative that manifests itself more harshly than in the case given by Eq.(34). The result is that the $h(t)$ waveform is more difficult for the algorithm to approximate as seen in Figure 12. The approximated waveform follows the true waveform well; however, it contains more unnatural oscillations.

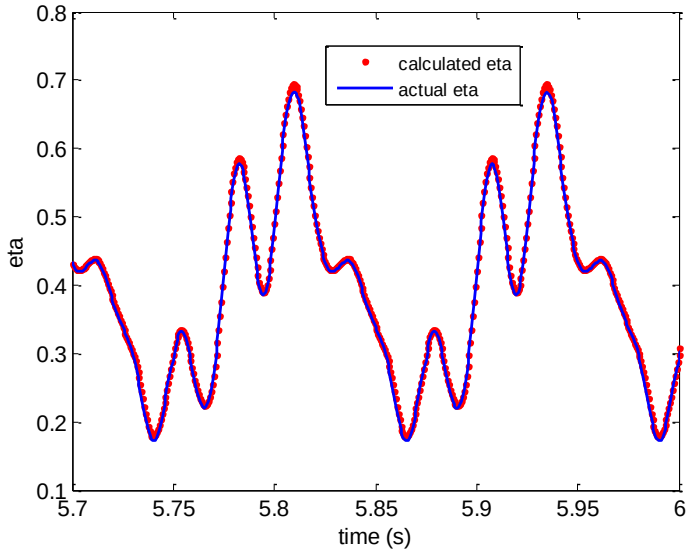

Figure 11: $\eta(t)$ WAVEFORM DETERMINED WITH 20 SECOND SIMULATED EXPERIMENT WITH WAVEFORMS GIVEN BY EQS. (36) AND (37)

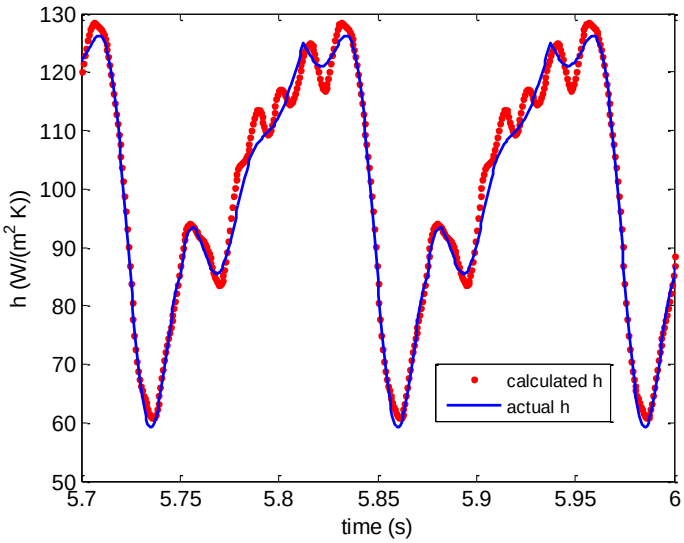

Figure 12: $h(t)$ WAVEFORM DETERMINED WITH 20 SECOND SIMULATED EXPERIMENT WITH WAVEFORMS GIVEN BY EQS. (36) AND (37)

HANDLING IMPERFECT STEP CHANGES

In the preceding analysis, we assumed perfectly instantaneous placement of the film cooled model in the wind tunnel. In a real experiment, there would be some amount of time that is required for the freestream temperature to reach its steady state value; a true step change is impossible to achieve in a laboratory. We now consider how the experimentalist may account for this in the data processing.

We assume that the model is held initially at the coolant temperature and coolant flows through the model at an already-constant temperature. Freestream air at a higher temperature is

turned on, but due to heat transfer taking place within the wind tunnel, the temperature ramps up to its final temperature over a finite period of time.

As discussed in the introduction, the invariance of η for a given set of flow conditions (identified through the Reynolds number and blowing ratio), irrespective of temperature, is a fundamental assumption in film cooling research. In other words, η is a function of the flow conditions, not an experiment's freestream and coolant temperatures. These temperatures are chosen for experimental reasons, such as measurement uncertainty or equipment limitations, but they do not change η. This invariance of η allows measurements made in the laboratory at temperatures cooler than engine temperatures to have practical application. Since η matches for the range of temperatures between a laboratory experiment and an actual engine, it certainly matches for small changes in T_∞ that occur over the course of an experiment.

Assuming the velocity field immediately assumes its steady-state periodic condition after test initiation, the $\eta(t)$ waveform must therefore also reach its steady-state periodic condition immediately, even though $T_{aw}(t)$ does not due to thermal transients. In the special case of steady film cooling, this translates to a constant value of η, but a value of T_{aw} that asymptotically approaches its final value. This assumption will not be completely accurate in a physical experiment because there is always a short amount of time during startup when the flowfield transitions to steady state. However, the aerodynamic transition to steady freestream flow should be, and in most cases is, very fast compared to the temperature transition.

In the discussion of the IFSAW algorithm earlier, we described a technique to find a periodic function $T_{aw}(t)$ that satisfies Eq. (27). For the more general case described here in which T_∞ is allowed to ramp up over time, $T_{aw}(t)$ is not a steady-state periodic function for the entire course of the experiment. Instead, we must use the fact that $\eta(t)$ is at a steady-state periodic condition throughout. This is an implicit advantage of using IFSAW over Eq. (16) for any time-varying flow conditions: IFSAW does not require constant T_{aw}, but only a velocity field which reaches periodic steady state quickly.

To use IFSAW in this configuration, we generalize Eq. (1) to account for the sources of unsteadiness, including in T_∞:

$$\eta(t) = \frac{T_\infty(t) - T_{aw}(t)}{T_\infty(t) - T_c} \tag{38}$$

Equation (27) can then be rewritten, eliminating T_{aw}:

$$q_s(t) = h(t)\left(T_\infty(t) - \eta(t)\left(T_\infty(t) - T_c\right) - T_s(t)\right) \tag{39}$$

We now wish to find the periodic function for $\eta(t)$ instead of $T_{aw}(t)$, using a procedure otherwise identical to that described earlier. Just as high frequency $T_s(t)$ measurements must be acquired, so too must $T_\infty(t)$ measurements. Similarly a filtering technique (such as Savitzky-Golay) would be appropriate for the $T_\infty(t)$ measurements to mitigate the effects of noise.

CONCLUSION

In this study, we developed and demonstrated a novel experimental technique and data reduction algorithm to determine the $\eta(t)$ and $h(t)$ waveforms from a transient film cooling experiment. The conduct of the experiment itself is identical to that used by Ekkad et al. [4]; however, the temperature data acquisition rate must be high enough to resolve the unsteadiness that is of interest to the researcher. Traditional data processing techniques with transient film cooling experimental data yield only single values for η and h. This is perfectly acceptable only when the flow is steady. The solution to the conduction equation used in the traditional technique assumes a constant convective boundary condition; any departure from that represents a misapplication of that technique. The new technique developed here allows for periodic fluctuations in η and h. Not only does the new technique allow for proper determination of $\bar{h}$ and γ, but it also allows temporal resolution of approximate $\eta(t)$ and $h(t)$ waveforms.

The views expressed in this article are those of the authors and do not reflect the official policy or position of the United States Air Force, the Department of Defense, or the US Government.

NOMENCLATURE

C	=	resistance to surface temperature fluctuations, $\sqrt{k\rho c\omega / (2\bar{h}^2)}$
c	=	specific heat, J/(kg K)
f	=	frequency, Hz
h	=	convective heat transfer coefficient, W / (m^2 K)
$\hat{h}_n$, $\tilde{h}_n$	=	coefficients in Fourier series for h, see Eq. (28)
k	=	thermal conductivity, W / (m K)
M	=	blowing ratio, $\rho_c U_c / \rho_\infty U_\infty$
N	=	number of summations in truncated Fourier series, see Eq. (28) and (29)
n	=	Fourier series index
q''	=	convective heat flux into a surface, W / m^2
t	=	time, s
T	=	temperature, K
$\hat{T}_n$, $\tilde{T}_n$	=	coefficients in Fourier series for T_{aw}, see Eq. (29)
x	=	distance into model material from surface, m
Δq_r	=	net heat flux reduction
α	=	thermal diffusivity, $k / (\rho c)$, (m^2/s)
ε	=	sum of the square of the errors or uncertainty
γ	=	unsteady coupled adiabatic effectiveness, $\gamma = \bar{\eta} + \overline{h_f' \eta'} / \bar{h}_f$
η	=	adiabatic effectiveness, (T_∞ - T_{aw})/(T_∞ - T_c)

ϕ	=	overall effectiveness, $(T_\infty - T_s)/(T_\infty - T_c)$, taken as independent of time
ρ	=	density, kg/m^3
ω	=	frequency, rad/s

Subscripts

0	=	without film cooling
aw	=	adiabatic wall
c	=	coolant
f	=	with film cooling
i	=	initial conditions
s	=	surface
∞	=	freestream recovery

Superscripts

$\bar{}$	=	temporal average
'	=	zero mean fluctuating component

REFERENCES

[1] Sen, B., Schmidt, D. L., and Bogard, D. G., 1996, "Film Cooling With Compound Angle Holes: Heat Transfer," ASME J. Turbomach., **118**, pp. 800–806.

[2] Rutledge, J.L., King, P.I., Rivir, R., 2010, "Time Averaged Net Heat Flux Reduction for Unsteady Film Cooling," ASME J. Engineering for Gas Turbines and Power, **132**, 121901.

[3] Vedula, R.P. and Metzger, D.E., 1991, "A Method for the Simultaneous Determination of Local Effectiveness and Heat Transfer Distributions in Three Temperature Convective Situations," ASME Paper No. 91-GT-345.

[4] Ekkad, S.V., Ou, S., Rivir, R.B., 2004, "A Transient Infrared Thermography Method for Simultaneous Film Cooling Effectiveness and Heat Transfer Coefficient Measurements from a Single Test," ASME J. Turbomach., **126**, pp. 597-603.

[5] Incropera, F., and DeWitt, D., 1996, *Fundamentals of Heat and Mass Transfer*, 4th ed., John Wiley & Sons, New York.

[6] Özisik, M.N. and Orlande, H.R.B., 2000, *Inverse Heat Transfer*, Taylor & Francis, New York.

[7] Savitzky, A. and Golay, M.J.E., 1964, "Smoothing and Differentiation of Data by Simplified Least Squares Procedures," *Analytical Chemistry*, **36**, pp. 1627–1639.

[8] Anderson, John D., 1995, *Computational Fluid Dynamics-The Basics with Applications*, McGraw-Hill.

[9] Carslaw, H.S., and Jaeger, J.C., 1986, *Conduction of Heat in Solids*, 2nd ed., Oxford University Press.

[10] Keith, F., 1998, *The CRC Handbook of Mechanical Engineering*, CRC Press.

[11] Rutledge, J.L., 2009, "Pulsed Film Cooling on a Turbine Blade Leading Edge," Ph.D. Dissertation, Department of Aeronautics and Astronautics, Air Force Institute of Technology, Wright-Patterson AFB, OH.